University of Baghdad
College of Engineering
JE
JOURNAL OF ENGINEERING

Journal of Engineering

journal homepage: www.jcoeng.edu.iq

Number 8 Volume 24 August 2018

Mechanical and Energy Engineering

Experimental and Numerical Analysis of Expanded Pipe using Rigid Conical Shape

Ahmed Ibrahim Razooqi
Assistant Lecturer
Engineering Technical College/Baghdad- Middle Technical University
Email: ahmed_air24@yahoo.com

Abstract

The experimental and numerical analysis was performed on pipes suffering large plastic deformation through expanding them using rigid conical shaped mandrels, with three different cone angles (15◦, 25◦, 35◦) and diameters (15, 17, 20) mm. The experimental test for the strain results investigated the expanded areas. A numerical solution of the pipes expansion process was also investigated using the commercial finite element software ANSYS. The strains were measured for each case experimentally by stamping the mesh on the pipe after expanding, then compared with Ansys results. No cracks were generated during the process with the selected angles. It can be concluded that the strain decreased with greater angles of conical shape and an increase in expansion ratio results in an increase of expansion force and a decrease in the pipe thickness and length resulting in pipe thinning and shortening. Good agreement is evident between experimental and ANSYS results within discrepancy (16.90017%) in the X direction and (27.68698%) in the Y direction. Also, the stress distribution is investigated and it can be concluded that the case of Diameter (D_o cone) = 35mm and (A) = α = 15° is the optimum.

Keywords: Solid tubular expansion, Expanded pipe, analytical model, finite element analysis, ANSYS.

التحليل العملي والعددي للأنبوب الموسع باستخدام شكل مخروطي مصمت

احمد ابراهيم رزوقي
مدرس مساعد
الجامعة التقنية الوسطى- الكلية التقنية – الهندسية بغداد

الخلاصة

تم إجراء التحليل العملي والعددي على الأنابيب التي تعاني من تشوه لدن كبير من خلال توسيعها باستخدام نموذج على شكل مخروطي مصمت، مع ثلاثة زوايا مخروطية مختلفة (15°، 25°، 35°) وأقطار (15، 17، 20) ملم. تم اشتقاق النموذج العملي للتنبؤ بنتائج الانفعال في المناطق الموسعة. كما تم البحث عن حل عددي لعملية توسيع الأنابيب باستخدام برنامج الأنسيس الخاص بالعناصر المحددة. حيث تم قياس الانفعالات لكل حالة عملياً عن طريق ختم شبكة على الأنابيب قبل وبعد التوسع، ثم المقارنة مع نتائج الأنسيس. لم يتم إنشاء أي تشققات أثناء العملية مع الزوايا المحددة. ويمكن استنتاج أن الانفعالات انخفضت مع زوايا أكبر من الشكل المخروطي وزيادة في نسبة التوسع يؤدي إلى زيادة قوة التوسع وانخفاض في سمك الأنابيب والطول مما أدى إلى ترقيق الأنابيب وتقصيرها. هنالك توافق جيد واضح بين النتائج العملية و الأنسيس ضمن التناقض باتجاه X هو (16.90017%) و باتجاه Y هو (27.68698%). ايضاً يمكن ملاحظة أن افضل أجهاد مكافئ كان عند الحالة بقطر 35ملم وزاوية (15°) هي المثلى.

*Corresponding author
Peer review under the responsibility of University of Baghdad.
https://doi.org/10.31026/j.eng.2018.08.09

Article accepted: 31/10/2017

1. INTRODUCTION

Experimental, numerical and analytical solutions of pipes have attracted the attention of many researchers in both theoretical and applied sciences. There are many technical and industrial applications in which the pipes play an important role due to their high strength and geometric shape. They are widely used in aerospace, marine, military, automotive, oil and gas, and other industrial fields. One of the main applications is in the oil and gas industry, particularly in the oil-well casing. Using a rigid conical shaped core for pipe expansion is a process of plastic deformation of the material on the tapered part of the inserted object as in **Fig.1** to change the initial radius by extended pipe to the required value. **Tahseen, et al., 2015,** study included the influence of work hardening property which makes this study with a great importance in how to deal with this property. This study showed a good agreement between both theoretical and practical parts, especially in determining the relative forming stress necessary for the success of the operation that showed the relative forming stress increases as the expansion ratio and the semi-cone angle of the mandrel increases has ranged between (0.1-0.7) of the samples tested. Noting that the formation is influenced by the first was much larger than the second was. Whereas the relative forming stresses decrease as the relative thickness increases for the same expansion ratio and the semi-cone angle of the mandrel formation. **Fischer, et al., 2006** in their paper dealt with a metal forming process leading to a conical extension of circular cylindrical shells (tubes). This forming process is called ‘flaring’. Analytical expressions are derived for determining stress and strain fields as well as the force required for driving the expansion. The results are compared to finite element solutions and show reasonably good agreement**. Shakeri, et al., 2007**, studied theoretical solutions for the expansion of the wall of the pipes that were placed under the influence of different types of loading. **Karrech and Seibi**, **2010,** derived a model for predicting the stress in the expanded area. **Joseph and Jacob, 2003** and **Jialing, et al., 2010,** developed a process in which elastic-plastic behavior was addressed in thick-walled cylinders. **Seibi, et al.**, **2005**, concluded that there is a regular pressure between the pipe shape and rigid core during the expansion process. **Omar, 2011** and **Omar and Tasneem, 2013,** introduced theoretical and experimental solutions to predict the variation in both length and thickness of the pipe. **Venugopal, et al., 2017,** defined end forming as forming the end of tubular forms either by inverting the tube or by expanding it. It finds application in many fields such as in the automotive and aerospace sectors as power transmission elements, fuel lines, exhaust pipes etc. The main aim of the present work is to expand the AA2014 alloy tubes with different die sets without any fracture. Deform 2D software was used for performing simulations on expanding the tubes with different die set (punch) values having different forming angles (α =15°, 30°, and 45°) and expansion ratios (rp/r0 =1.39, 1.53 and 1.67). In the previous papers, the relation between the angle of cone and stress are not investigated, so this paper, several sizes of pipe are used with a different configuration, like outer diameter of cone mandrel (15,17, and 20) mm with different mandrel angles (15°,25°, and 35°) respectively and found the strain distribution for each case.

2. NUMERICAL SIMULATIONS

Simulating of the three different cone angles (15°, 25°, and 35°), were investigated using three diameters for mandrel cones in the values of (15, 17, and 20) mm. Commercial FEA software ANSYS 15 was used; the stroke steps on rigid cones were defined explicitly over a time span. Within each step, several solutions (sub-steps or timesteps) were performed to apply the pressure gradually. At each sub-step, a number of equilibrium iterations were performed to obtain a converged solution, ANSYS 15.0, User guide, 2015.

The solid coned-head was modeled as a rigid body. Contact procedure in ANSYS 15 was used to model the complex interaction between the pipe and cone, the 2D contact element TARGE169 was used, to represent 2D (cone set) surfaces which were associated with the deformed body (pipe) represented by 2D contact elements of CONTA175. “mandrel profile” shown in **Fig. 2-A-B** was designed depending on the pipe diameter illustrated in following D_o= 12.7,16 and 19mm.

(Element PLANE182) was used for 2-D modeling of solid structures that are shown in **Fig. 2**. The element can be used as either a plane element (plane stress, plane strain or “generalized plane strain”) or an axisymmetric element. It is defined by four nodes having two degrees of freedom at each node, translations were in the nodal x and y directions. The “element” was considered to have plasticity, hyperelasticity, stress stiffening, large deflection, and large strain capabilities Johnson K.I.et al 2004.

Most elements types require material properties. Depending on the application, they may be taken as **Nakasone and Yoshimoto, 2006:**

- Linear or nonlinear.
- Isotropic, orthotropic, anisotropic.
- Constant temperature or temperature-dependent.

The Pipes material is copper and its properties were determined experimentally with a coefficient of friction as 0.15 **Ibraheem, 2006**. The plastic response was modeled using the Von Mises yield criterion. The element shape was specified, mapped and meshed, as in **Fig. 3** which shows the meshing. This stage is important as it is the step by which the geometrical model is converted to a finite element model (FEM).

In studying the contact between two bodies, the surface of the first one is conventionally taken as a contact surface while the other is considered as a target surface. The “contact -target” pair concept has been widely used in finite element simulations**, ANSYS 15, 2015.** For rigid-flexible contact, the “contact surface” is associated with the deformable body; and the “target surface” must be the rigid surface. For flexible-flexible contact, both contact and target surfaces are associated with deformable bodies. The contact and target surfaces constitute a **“**contact Pair**”.** ANSYS supports both rigid-to-flexible and flexible-to-flexible surface-to-surface, contact elements, which were used as "target surface" and a "contact surface" to form a contact pair. The target surface is modeled with TARGE169 or TARGE 170 (for 2-D or 3-D, respectively), **Johnson, 2004.**

3. EXPERIMENTAL PART

3.1 Chemical Composition Test

The specimen material used is copper of commercial standards - ASTM B280 - C11000 **Volume, ASM Handbook**, **1990** and its purity was determined by spectrometer analysis via atomic absorption and found to be 99.91 copper, **Table 1** illustrates the chemical composition of material and **Fig. 4** represents the chemical composition apparatus in the (Standardization and Quality Control Device).

3.2 Pipe Material Properties

In order to determine the mechanical properties of the copper pipe, a tensile test was performed with the dimensions illustrated in **Fig. 5** where (d) =16.8mm and gauge length = (4d). **Fig. 6** shows the dimensions of the specimen as given by the (**Standard Test Methods for Tension Testing of Metallic Materials 2015. Fig. 7** illustrates the stress-strain curve from which the important mechanical properties of pipe material were obtained which can be used in numerical and experimental tests like yield stress, modulus of elasticity, ultimate stress and tangent modulus all shown in **Table 2**, the experiments were conducted in the (Institute of Technology / Baghdad, Mechanical Department).

3.3 Expanding Pipe Test

In this work, copper pipes, as described in **Table 2**, were tested as a model for the pipe expansion process, where sets of three mandrels, were designed and manufactured on the basis of different variables (diameters and angles). Lubricants were used for the purpose of obtaining the best results in the expansion of the sample pipes. The dies were manufactured with diameters of

(D_O = 15mm, D_O = 20mm and D_O = 17mm). Three angles (15^o, 25^o, 35^o) were taken for each diameter, so the total number of dies were 9 by 3 angles per-diameter. A bar saw as well as a turning machine was used for manufacturing and experimentation. Practical tests were carried out by taking samples with the prerequisite copper pipes to be expanded to the present diameters and angles with the use of lubricants for smoothness and easiness of formation during the experiment. The samples were mounted on a fixture well grabbed by the chuck of the turning machine while the mandrel is inserted in a steady, gradual, and linear movement from the other side, as can be observed in **Fig. 8**, to reach the required formation and expansion to the inner diameter of the pipe.

3.4 Strain Measurement Test

The pipe was screened with an initial grid measurement of **(5 *5)** mm, and after the test it can be apparent that the length of the grid had changed while the deviation was measured by the AutoCAD program to find the change in the length, (insertion the picture of grid spacemen with rural and making scale to the picture using reference point after that the distance is measured between two points in the grid which represent the change in length). Then the strain is determined, as the image was inserted and scaled then the change of the dimensions in the length of the grid was calculated as showing **Fig. 9**.

4. RESULTS AND DISCUSSION

Fig 10 illustrates the strain in (X) axis with $D_{o\ Cone}$ = 15mm with α = 15°, 25°, and 35° respectively. Where **Fig. 10-a** shows that the strain increases firstly and then decreases within a distance interval of 10-20 mm then rises again till the end. **Fig. 10-b** had similar behavior while **Fig. 10-c** indicates an increase in the strain at first then becomes approximately constant. Good agreement is evident between Ansys results and experimental results. The discrepancy being (15.71186%).

Fig. 11 demonstrates the behavior of the strain in the (X) axis having $D_{o(Cone)}$=17mm with α=15°, 25°, and 35°cnsecutively. In **Fig. 11-a** the curve goes approximately constant, till the of distance 25mm then increases up to the end. While **Fig. 11-b** shows that strain increases sharply then remains constant for a distance range of (10-20) mm after which it declines to the end. **Fig. 11-c** the strain takes the trend of dropping down and rising again two times with the point of 20mm being in the middle between those two parts. Again, the Ansys results prove little difference from the practical ones as the discrepancy factor is 15.55882%.

Fig. 12 represents the strain in the (X) axis with Do_{cone} = 20mm while α=15°, 25°, and 35°. Part A is showing increasing and decreasing in a zigzag rhythm within a period of approximately 10mm starting from 5 mm and ending at 30mm. Parts B and C have approximately the same behavior as in the previous case. The Ansys analysis and the experimental results are almost identical. The discrepancy is (19.42984%).

It can be noticed in **Fig. 13** that the (Y) axis resembles the strain with ($D_{o\ cone}$ =15mm) and the same values for α as in the above cases. It is clear that in **Fig. 13-a** the strain is increasing at first before decreasing in an interval of 10-20mm to return to rising finally. **Fig. 13-b** shows that the curve takes a (V) shape from a strain value of up 0.06 to the lowest point of 0.007 in a of period 10-20mm. **Fig. 13-c** shows a Bell-like distribution of date for a distance range of (5-15) mm, and from a peak of 0.095 to a bottom of 0.01 strain values. The theoretical analysis is in good coordination with the practical results. The discrepancy is (25.77037%).

Fig. 14 representing the strain on the (Y) axis having $D_{o\ cone}$ being (17mm) and α is taken as 15°, 25° and 35° for each case. **Fig. 14-a** shows the strain to be almost constant within the distance between 5-20mm to rise to a peak of 0.12 then declining to 0.01 at the end, while **Fig. 14-b** behavior to be of almost fixed value till the point of 15mm where it drops sharply to 0.05 then return to its starting value of 0.1 at the end. For the third condition in **Fig. 14-c,** the curve shows a gradual and almost steady decrease from 0.12 at the beginning (point 5mm) to 0.02 at the finish (distance +30mm). The discrepancy is (35.59921%).

Finally, in the case of Do $_{cone}$ =20mm with the same three values of α as in all other experiments, **Fig. 15** illustrates the strain in (Y) axis, where, as in **Fig. 15-a**, it starts as almost constant at values ranging close to (0.1-0.12), and within the distance between (5 and 20) mm, then plunges down to 0.04 to rise a little at the end. **Fig. 15-b** shows that the strain decreases dramatically by about 0.07, in the interval of (5mm) starting at the distance of 5mm, then increases sharply within the period of 15-20mm, lastly it takes another small v shape to end at about (0.8). In **Fig. 15-c** it can clearly be noticed that the strain begins from its low range of values (0.015-0.03) to rise fast to its peak, within the period 15-20mm, then decline a little before increasing slightly again at the end. Almost identical alignment is clear between theoretical and true values. The discrepancy (21.69136%).

From the above figures, the increased and decreased curves in the points of deformed shape is happening by generation the tension and compression stresses in the formed region that caused the metal flow in the plastic zone which is the nonlinear zone, so increasing and decreasing appeared in the response.

The variation in the strain caused is due to friction forces with the pipe wall because of the applying load. Also, it can be concluded that the strain in the X and Y-axis decreased with increasing the angle of conical shape. An increase in expansion ratio results in an increase of expansion force and a decreasing in the pipe thickness and length resulting in pipe thinning and shortening. The average discrepancy between the experimental and numerical results is (16.90017%) in the X direction and (27.68698%) in the Y direction. **Figs 17, 18, 19, 20, 21,** and **22** show the strain distribution in the X and the Y axis at the various conditions of experimentation.

Figs 22, 23, and **24** show the equivalent stress distribution in the X and the Y axis at the various conditions of experimentation. It can be observed that Diameter (D_o cone) = 35mm and (A) = α = 15° had the less equivalent stress, i.e. this case is the optimum.

5. CONCLUSIONS

1- Good agreement is evident between experimental and ANSYS results within a discrepancy of (16.90017%) in the X direction and (27.68698%) in the Y direction.
2- The strain decreases with greater angle of the conical shape.
3- The higher the expansion ratio, the greater the expansion force, but with lesser pipe thickness and length.
4- It can be concluded that the case of Diameter (D_o cone) = 35mm and (A) = α = 15° is the optimum.

6. REFERENCES

- ANSYS 15.0, 2015, User guide.
- Fischer, F.D., Rammerstorfer, F.G. & Daxner, T., 2006, Flaring- an Analytical Approach, International Journal of Mechanical Sciences 48, 1246-1255.
- Ibraheem T. Hussain, 2006, Manufacturing and Analysis of Components Using Bulging Forming: Tube Hydroforming Processes, M.Sc. thesis AL-Nahrain University.
- Jialing Yang, Min Lou, Yunlong Hua, and Guoxing Lu, 2010, Energy Absorption of Expansion Tubes Using a Conical Cylindrical Die: Experiments and Numerical Simulation., International Journal of Mechanical Sciences 52 ,716-725.

- Johnson K.I., Nguyen B. N., Davies R.W., Grant G.J., and Khaleel M.A., 2004, A Numerical Process Control Method for Circulartube Hydroforming Prediction, International Journal of Plasticity, Vol. 20, pp 1111–1137.
- Joseph Perry and Jacob Aboudi, 2003, Elasto-Plastic Stresses in Thick Walled Cylinders, Journal of Pressure Vessel Technology, AUGUST, Vol.125, pp.248-252.
- Karrech, A. and A. Seibi, 2010, Analytical Model for the Expansion of Tubes under Tension, Journal of Materials Processing Technology 210, 356-362.

- Nakasone Y. and Yoshimoto S., 2006, Engineering Analysis with ANSYS Software, Department of Mechanical Engineering, Tokyo University of Science.
- Omar S. AL-Abri, 2011, Analytical and Numerical Solution for Large Plastic Deformation of Solid Expandable Tubular, SPE paper # 152370- STU Colorado, USA, 30 October- 2 November.
- Omar S.AL -Abri, and Tasneem Pervez, 2013, Structural Behavior of Solid Expandable Tubular Undergoes Radial Expansion Process- Analytical, Numerical, And Experimental Approaches, International Journal Solids and Structures 50, 2980- 2994.

- Seibi, A.C., Al-Hiddabi, S., Pervez, T., 2005, Structural Behavior of a Solid Tubular under Large Plastic Radial Expansion, ASME Journal of Energy Resources and Technology 127, 323–326.
- Shakeri, M., Salehghaffari, S. and Mirzaeifar, R., 2007, Expansion of Circular Tubes by Rigid Tubes as Impact Energy Absorbers, Experimental and Theoretical Investigation, TCRS Vol.12 No.5, pp.493-501.

- Standard Test Methods for Tension Testing of Metallic Materials, 2015, Designation: E 8, American Association State, Highway and Transportation Officials Standard, AASHTO No.: T68, An American National Standard.
- Tahseen Taha Othman, Hazim Khalil Khalaf, and Jalal Khorshed Alyan, 2015, Experimental Study of Steady-State Tube Expansion by using Conical Mandrel, the number. (A) Journal of Engineering and Technology, vol. 33.
- Venugopal, L, Prasad, N E C, Geeta Krishna, P, and Praveen, L, 2017, Simulation Studies on Tube End Expansion of AA2014 Alloy Tubes, (ICRAMMCE), 31 May.

- Volume, ASM Handbook, 1990, 2: Properties and Selection: Nonferrous Alloys and Special-Purpose Materials, ASM international, pp 889-896.

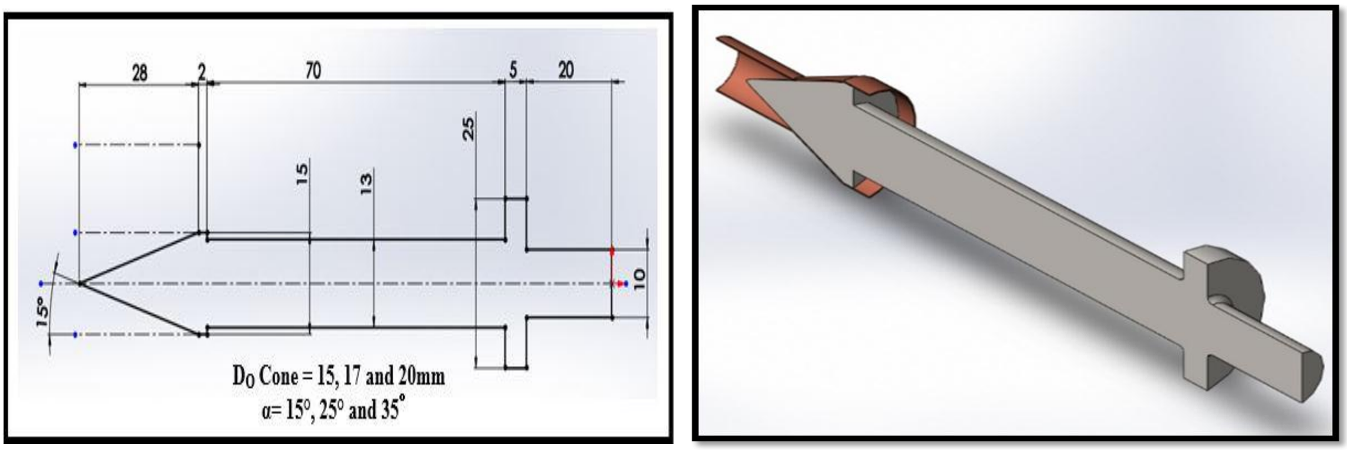

A B

Figure 1. Mandrel die profile configuration. (A) dimensions of rigid profile (B) section of rigid pipe.

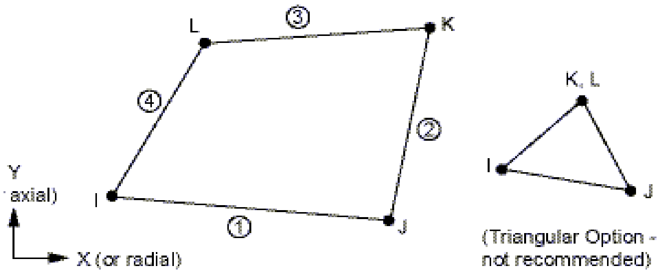

Figure 2. Plane 182 geometry.

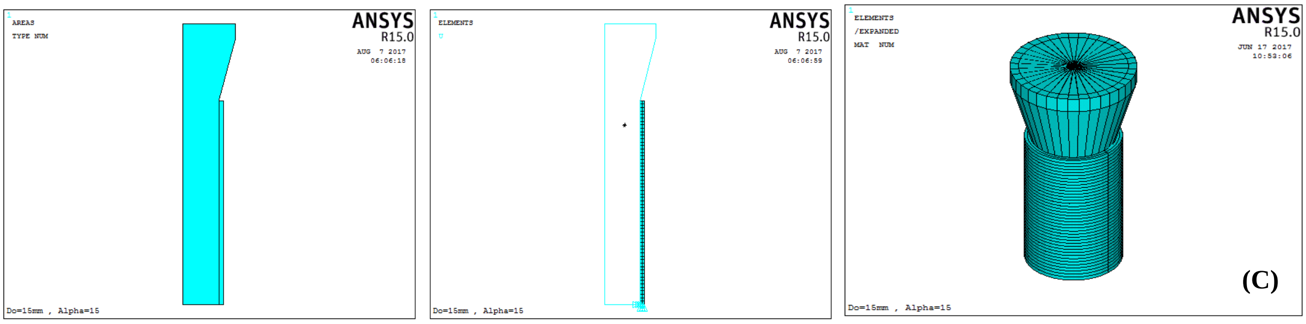

Figure 3. A- axisymmetric drawing, B-axisymmetric Boundary condition, C-full modal

Table 1. The chemical composition of copper pipe

Elem.	Cu	Zn	Pb	Sn	P	Si	S	As	Ag	Bi	Cd	Sb	Se	Te	Au
Expr.	99.91	0.008	0.003	0.008	0.019	0.013	0.005	0.007	0.003	0.002	0.001	0.008	0.0001	0.006	0.004
Stand.	99.90	-	-		-	-	-	-	-	-	-	-	-	-	-

Figure 4. Atomic Absorption Spectroscopy.

Figure 5. Tensile Test Machine and specimen.

Table 2. The mechanical properties of the copper pipe.

Modulus of Elasticity (E)	124GPa
Tangent Modulus of Elasticity (E_T)	0.8 E GPa
Yield Stress (σY)	105 MPa
Ultimate tensile	203.8Mpa
Poisson's Ratio (υ)	0.34

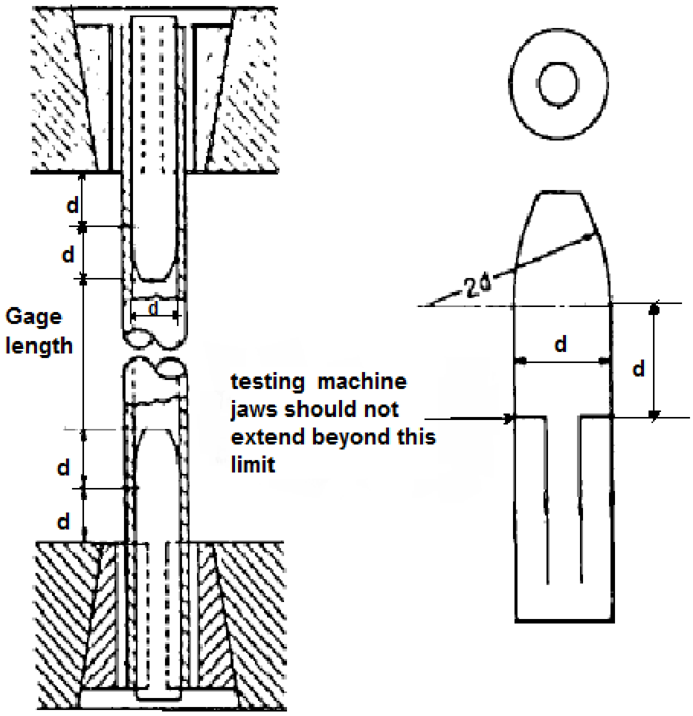

Figure 6. Dimensions of the specimen.
(d=16.8 and gauge length = 4d)

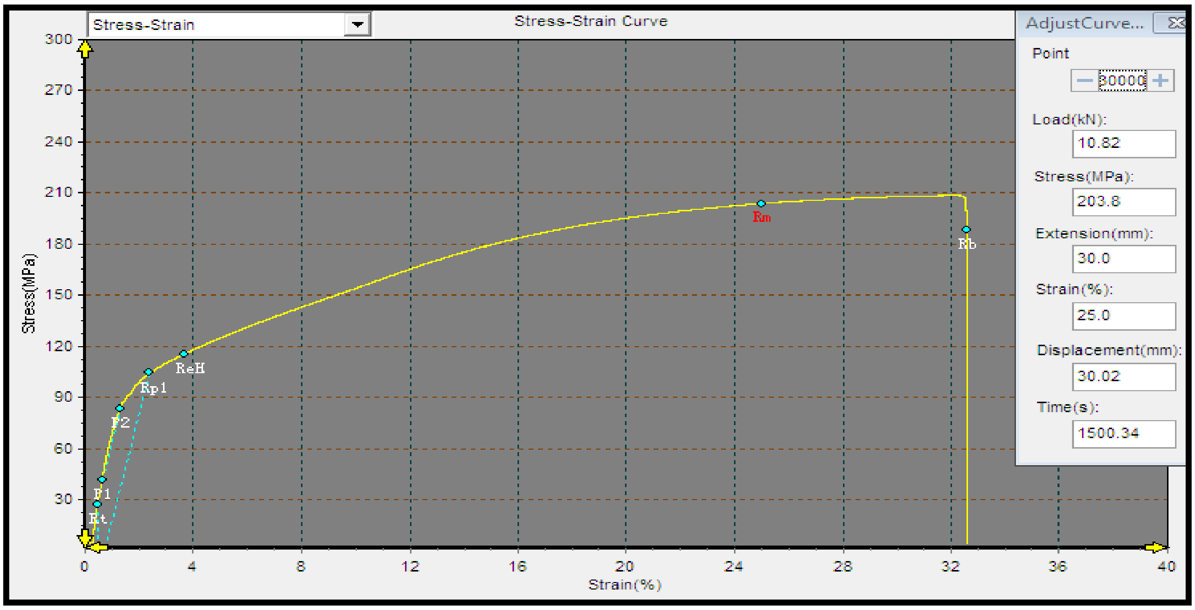

Figure 7. Engineering Stress-Strain curve for the copper pipe.

Figure 8. Steps for expanding pipe.

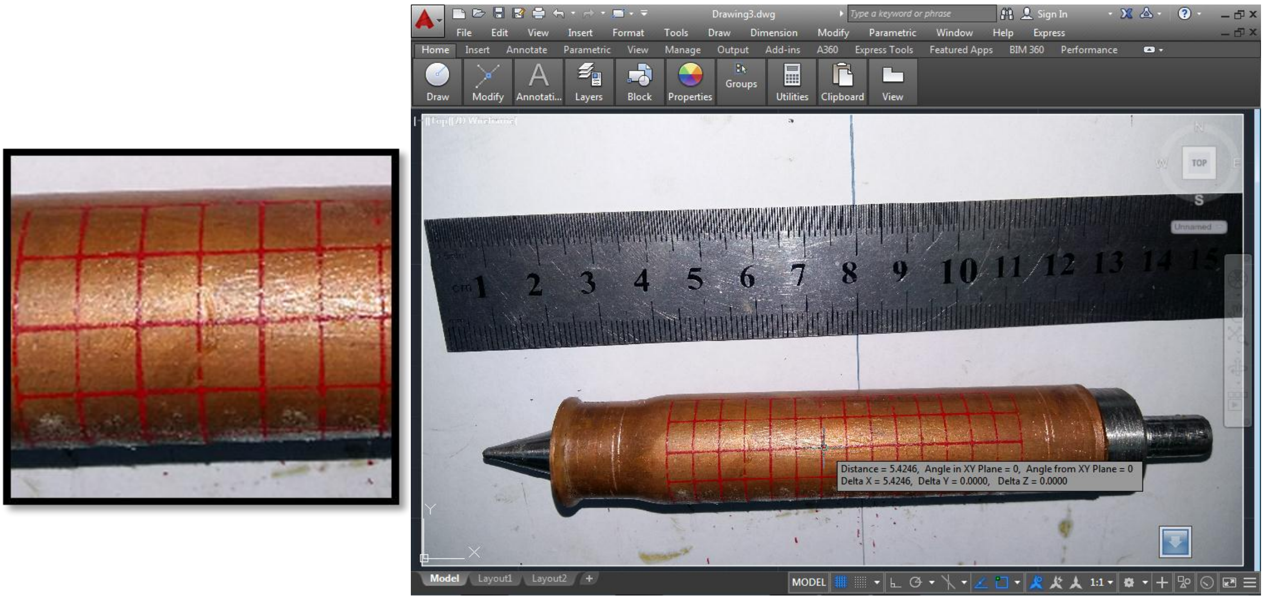

Figure 9. Measurement of changing the length of the grid.

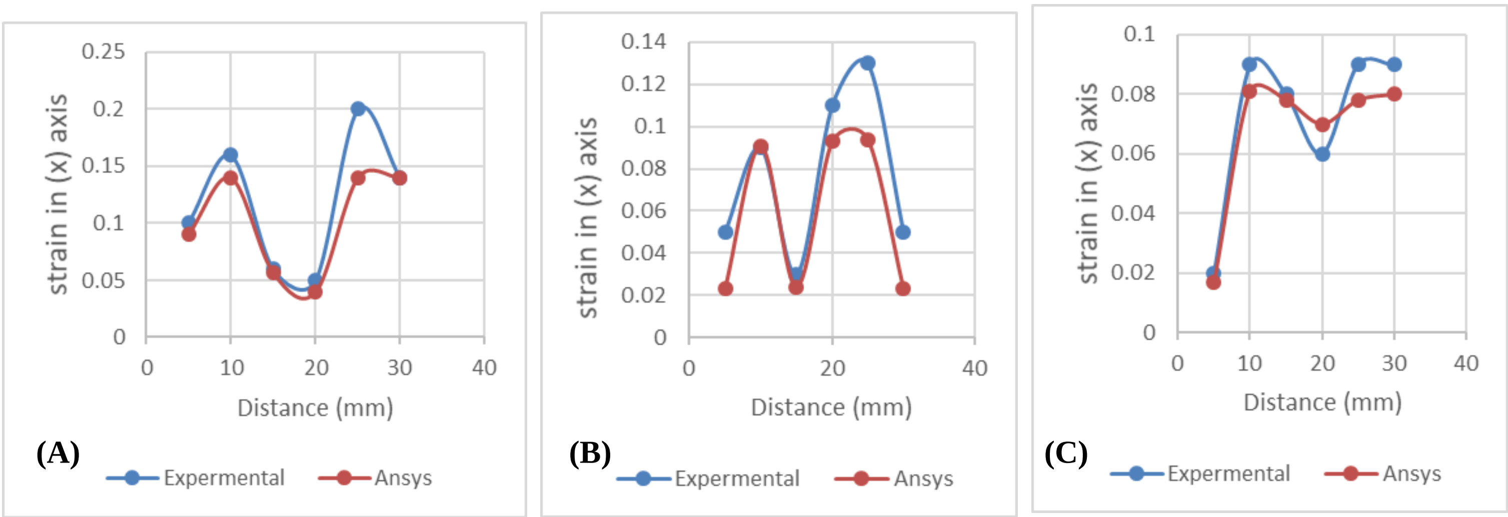

Figure 10. Pipe strain in (X) axis with $D_{o\ cone}$ =15mm and (A)=α=15°, (B)=α=25°, (C) =α=35°

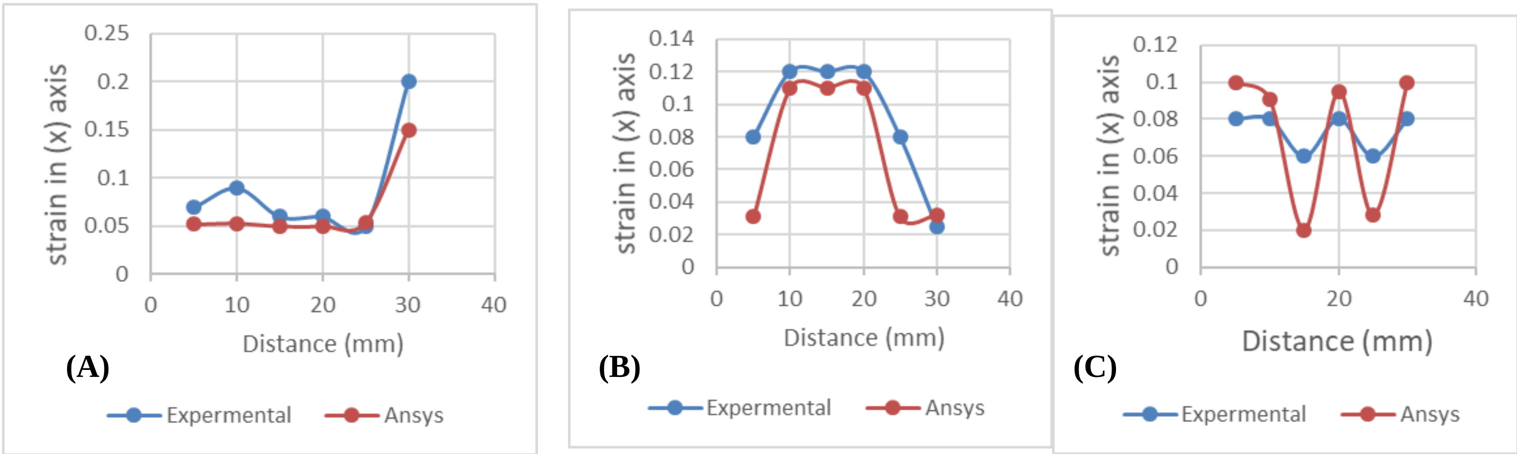

Figure 11. Pipe strain in (X)axis with Do cone =17mm and (A)=α=15°, (B)=α=25°, (C)=α=35°

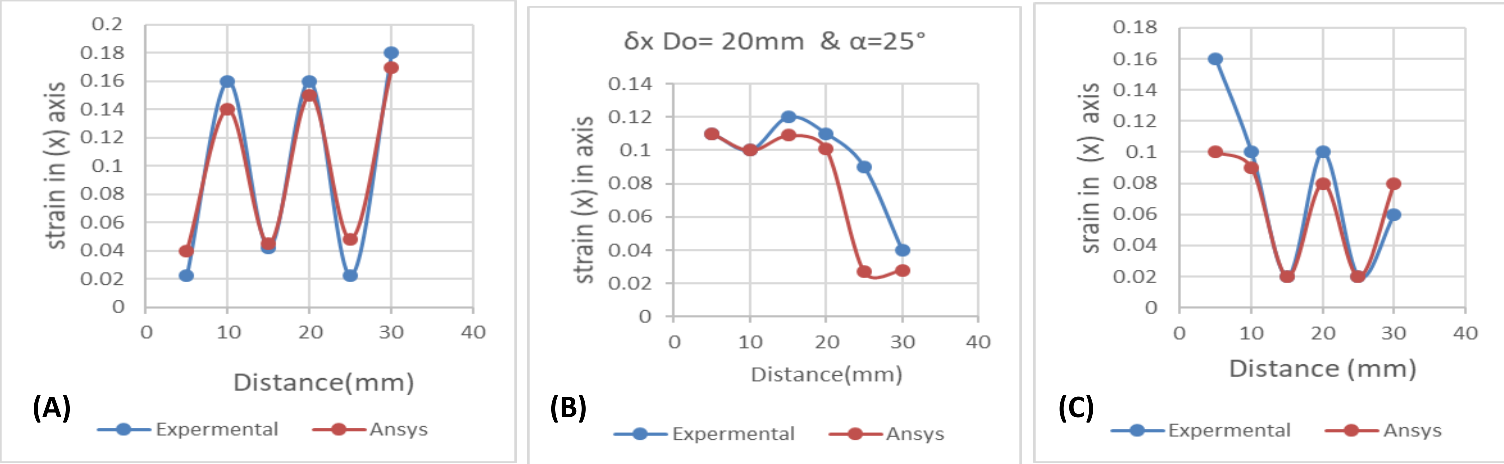

Figure 12. Pipe strain in (X) axis with $D_{o\ cone}$ =20mm and (A)=α=15°, (B)=α=25°,(C)=α=35°

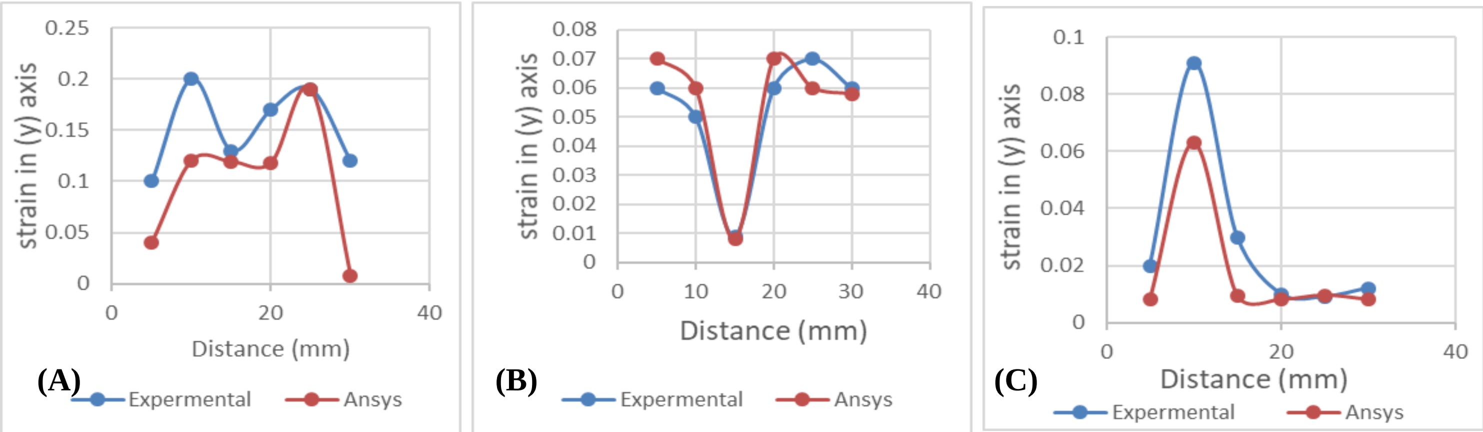

Figure 13. Pipe strain in (Y) axis with D_o cone=15mm and (A)=α=15°,(B)=α=25°,(C) =α=35°

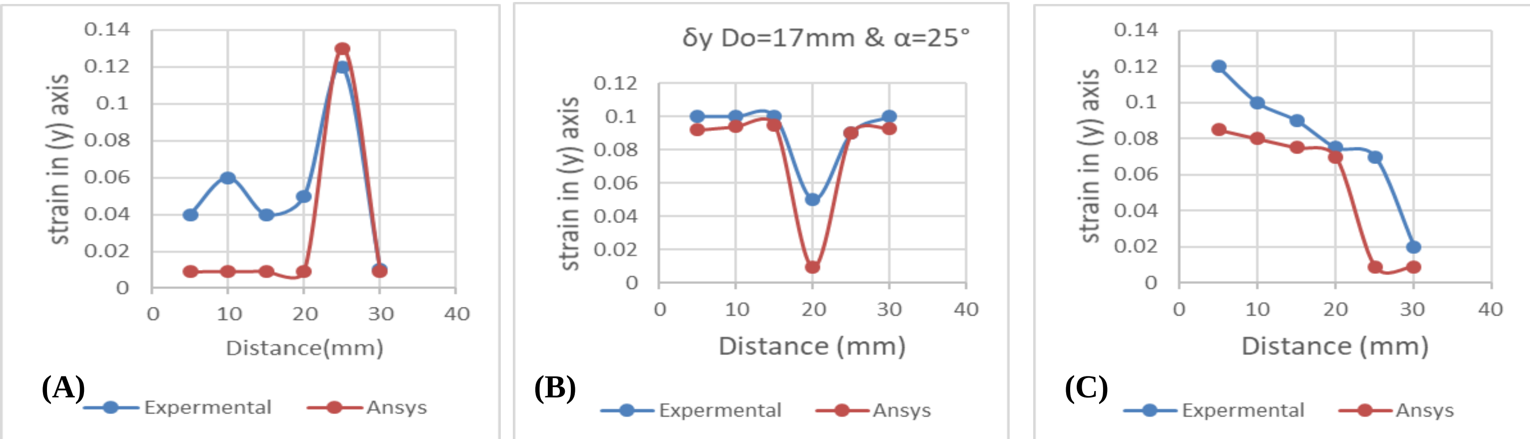

Figure 14. Pipe strain in (Y) axis with $D_{o\ cone}$=17mm and (A)=α=15°,(B)=α=25°,(C) =α=35°

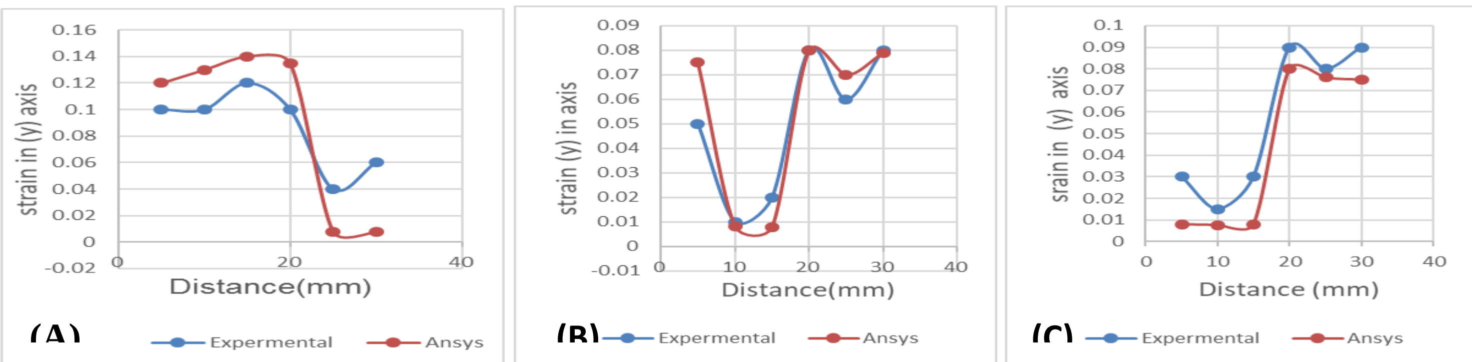

Figure 15. Pipe strain in (Y) axis with $D_{o\ cone}$=20mm and (A)=α=15°, (B)=α=25°, (C) =α=35°

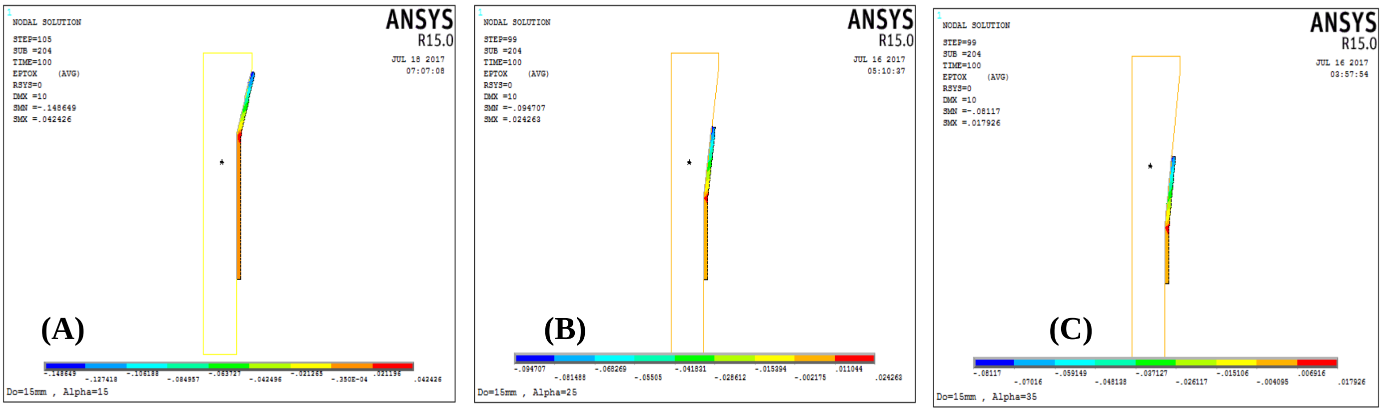

Figure 16. Pipe strain in (X) axis with $D_{o\ cone}$ =15mm and (A)=α=15°, (B)=α=25°, (C)=α=35°

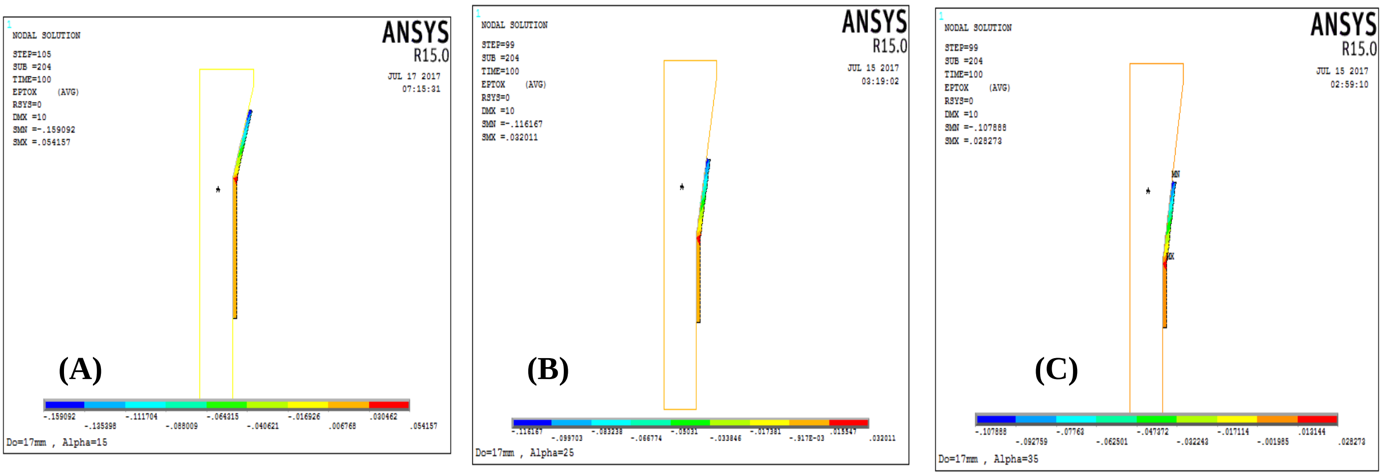

Figure 17. Pipe strain in (X) axis with Do cone =17mm and(A)==15°, (B)=α=25°, (C)=α=35°

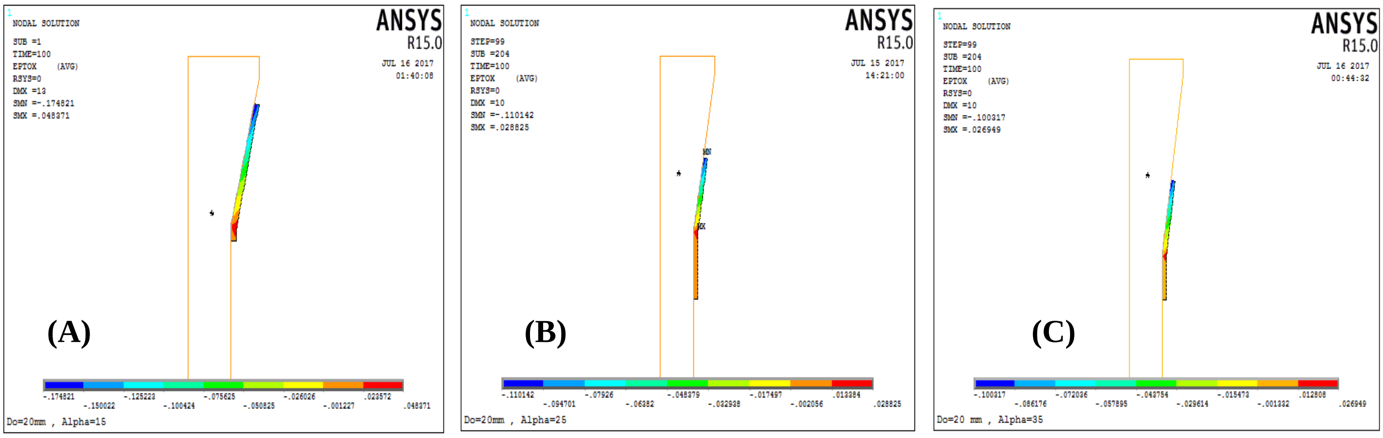

`**Figure 18.** Pipe strain in (X) axis with Do cone = 20mm and (A)=α=15°, (B)=α=25°,(C) =α=35°

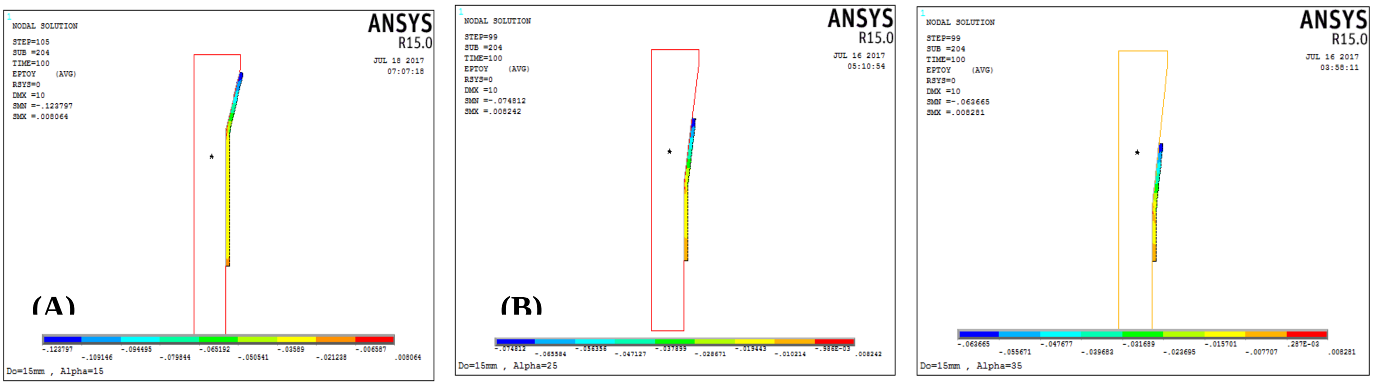

Figure 19. Pipe strain in (Y) axis with Do cone =15mm and (A)=α=15°, (B) =α=25°, (C)=α=35°

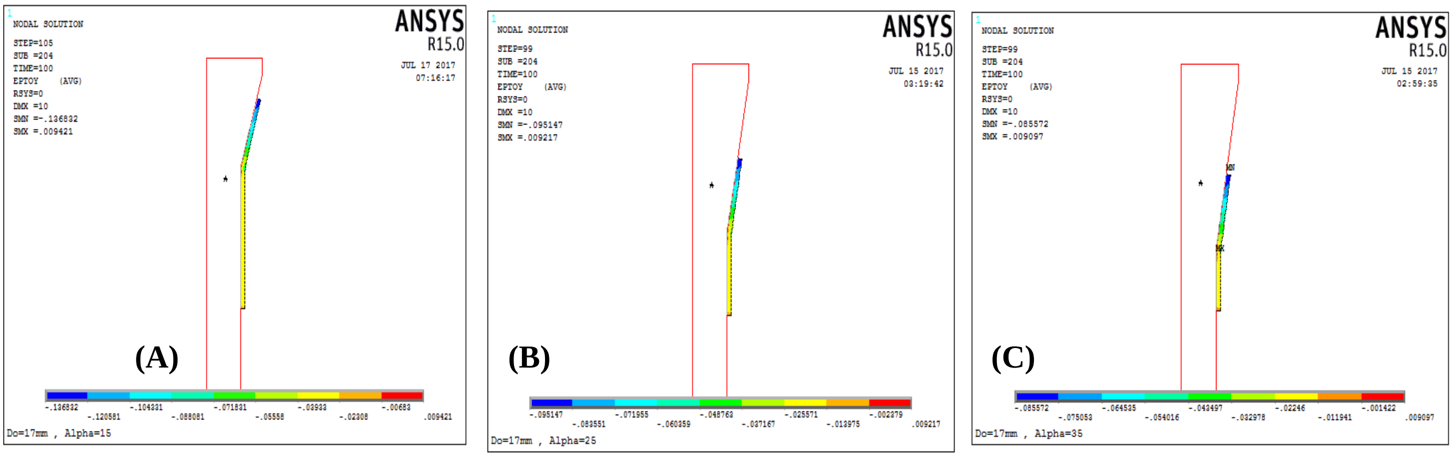

Figure 20. Pipe strain in (Y) axis with Do cone =17mm and (A) =α=15°, (B)=α=25°, (C)=α=35°

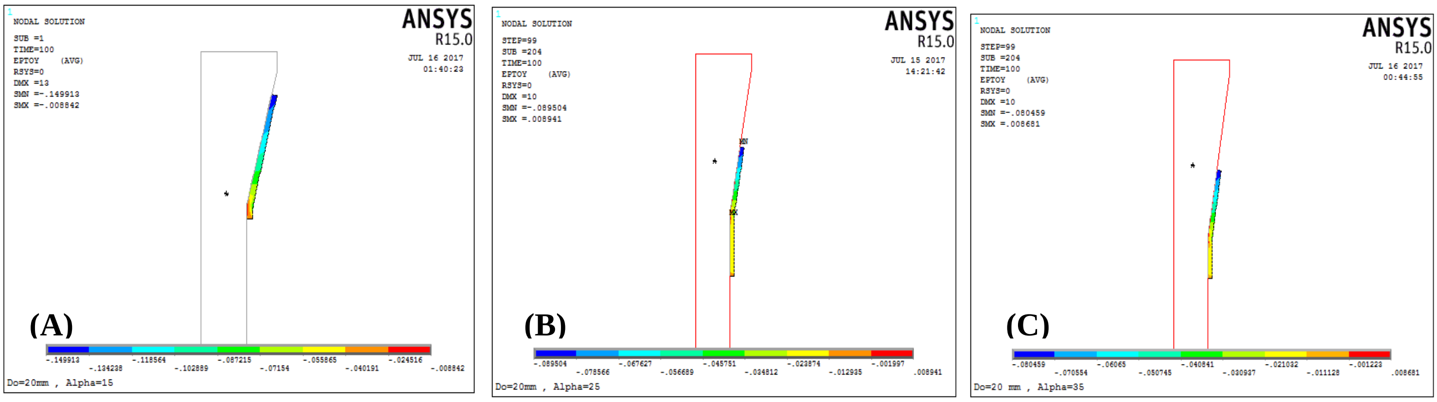

Figure 21. Pipe strain in (Y) axis with Do cone = 20mm and (A)=α=15°, (B)=α=25°, (C)=α=35°

Table 3. the equivalent stress distribution on X and Y axis at the various conditions of experimentation.

Diameter	**15mm**	**17mm**	**20mm**
Stress	**max. Equivalent Stress (MPa)**	**max. Equivalent Stress (MPa)**	**max. Equivalent Stress (MPa)**
Angle			
α=15°	20399.5	22697.4	24619.5
α=25°	12817.9	16020.6	15121.6
α=35°	10927.4	14414	13669.9

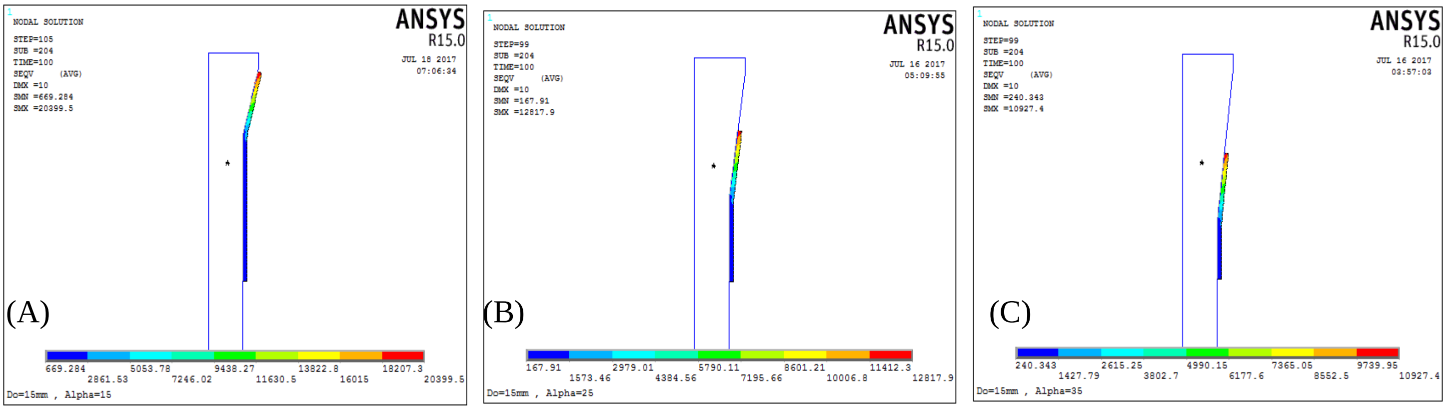

Figure 22. equivalent stress of pipe with D_o cone =15mm and (A)=α=15°, (B)=α=25°, (C)=α=35°

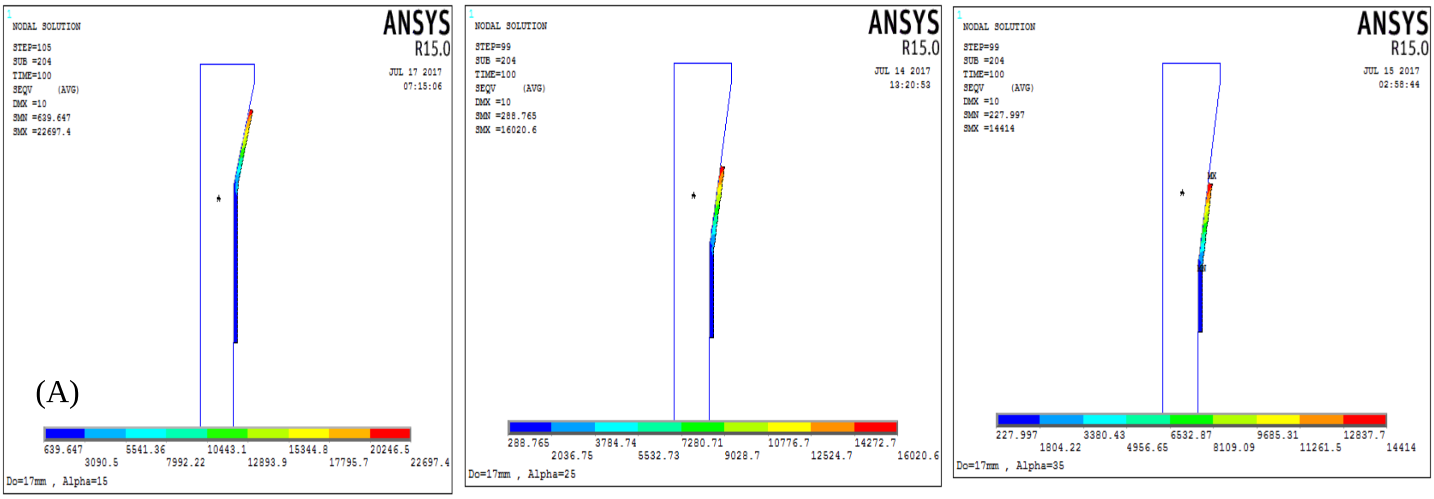

Figure 23. equivalent stress of Pipe with D_o cone =17mm and (A)=α=15°, (B)=α=25°, (C)=α=35°

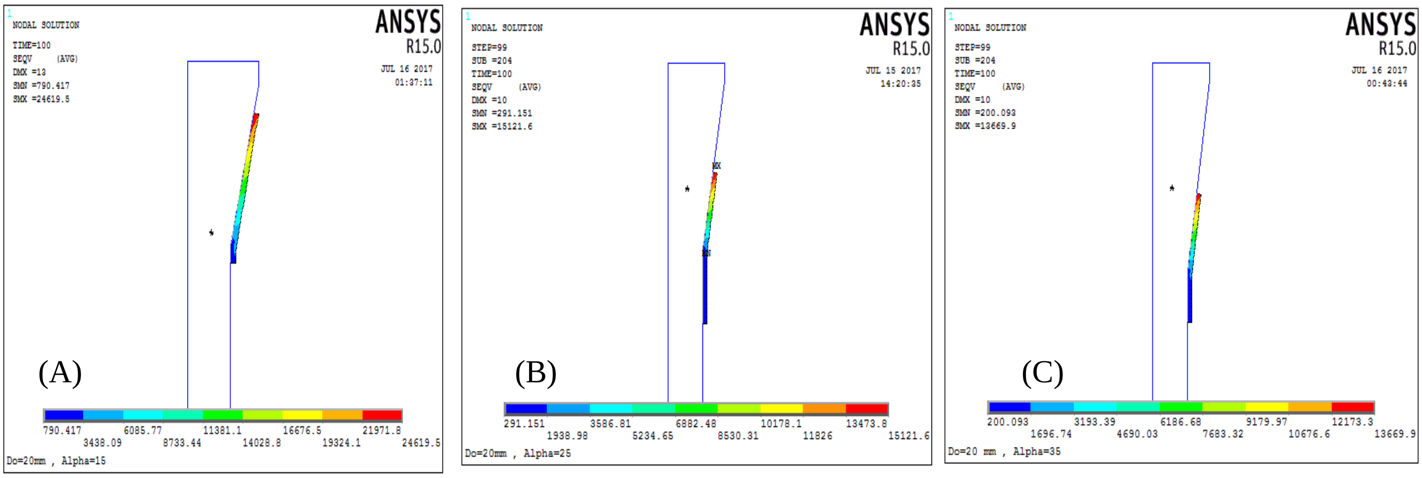

Figure 24. equivalent stress of Pipe with D_o cone =20mm and (A)=α=15°, (B)=α=25°, (C)=α=35°